Differences in *RAD51* transcriptional response and cell cycle dynamics reveal varying sensitivity to DNA damage among *Arabidopsis thaliana* root cell types

Konstantin Kutashev[1] (iD)**, Anis Meschichi[2]** (iD)**, Svenja Reeck[3]** (iD)**, Alejandro Fonseca[1]** (iD)**, Kevin Sartori[1]** (iD)**, Charles I. White[4]** (iD)**, Adrien Sicard[1]** (iD) **and Stefanie Rosa[1]** (iD)

[1]Plant Biology Department, Swedish University of Agricultural Sciences, Almas allé 5, Uppsala, 756 51, Sweden; [2]Department of Biology, Institute of Molecular Plant Biology, Swiss Federal Institute of Technology Zürich, Zürich, 8092, Switzerland; [3]Department of Cell and Developmental Biology, John Innes Centre, Research Park, Norwich, NR4 7UH, UK; [4]Institut Génétique Reproduction et Développement (iGReD), Université Clermont Auvergne, UMR 6293, CNRS, U1103 INSERM, Clermont-Ferrand, 63001, France

Author for correspondence:
Stefanie Rosa
Email: *stefanie.rosa@slu.se*

Summary

- Throughout their lifecycle, plants are subjected to DNA damage from various sources, both environmental and endogenous. Investigating the mechanisms of the DNA damage response (DDR) is essential to unravel how plants adapt to the changing environment, which can induce varying amounts of DNA damage.
- Using a combination of whole-mount single-molecule RNA fluorescence *in situ* hybridization (WM-smFISH) and plant cell cycle reporter lines, we investigated the transcriptional activation of a key homologous recombination (HR) gene, *RAD51*, in response to increasing amounts of DNA damage in *Arabidopsis thaliana* roots.
- The results uncover consistent variations in *RAD51* transcriptional response and cell cycle arrest among distinct cell types and developmental zones. Furthermore, we demonstrate that DNA damage induced by genotoxic stress results in *RAD51* transcription throughout the whole cell cycle, dissociating its traditional link with S/G2 phases.
- This work advances the current comprehension of DNA damage response in plants by demonstrating quantitative differences in DDR activation. In addition, it reveals new associations with the cell cycle and cell types, providing crucial insights for further studies of the broader response mechanisms in plants.

Introduction

Plants, due to their sessile nature, are constantly exposed to various DNA damaging agents from both the environment and endogenous processes. One of the most dangerous lesions that can occur on the DNA are double-stranded breaks (DSBs) (Vítor *et al.*, 2020). The occurrence of this type of lesions requires immediate repair, triggering DNA damage response (DDR) activation, recruitment of the DNA repair machinery to the lesion site, and cell cycle arrest until the repair is complete (Preuss & Britt, 2003; Cools *et al.*, 2011). In most cases, DSBs are repaired by one of two mechanisms: non-homologous end joining (NHEJ) or homologous recombination (HR) (West *et al.*, 2004). HR is typically regarded as an error-free repair system that relies on an intact DNA strand acting as a template for reconstruction of the broken DNA strand (Schuermann *et al.*, 2005).

Soon after the occurrence of a DSB, regions spanning thousands of kilobases around the newly formed DSB are labeled by phosphorylated form of H2A.X histone variant (γH2AX) that participates in the early signaling of the lesion and recruitment of DNA repair machinery proteins (Rogakou *et al.*, 1999; Stewart

et al., 2003; Lang *et al.*, 2012; Fan *et al.*, 2022). Histone γH2AX levels were shown to correlate with DNA damage amounts (Friesner *et al.*, 2005; Redon *et al.*, 2009; Lee *et al.*, 2019), and its dynamics of recruitment and loss are employed to measure DSB repair dynamics (Löbrich *et al.*, 2010; Lee *et al.*, 2019).

Homologous recombination pathway is intricately connected to the S and G2 phases of the cell cycle, owing to its inherent need for an intact repair template, with the sister chromatid predominantly serving this function (Johnson, 2000; Saleh-Gohari, 2004; Saintigny *et al.*, 2007; Goldfarb & Lichten, 2010; Bee *et al.*, 2013). This regulation is accomplished through cell cycle-linked transcriptional control of HR proteins and post-translational modifications of proteins during the S and G2 phases (Yata *et al.*, 2012; Weimer *et al.*, 2016; Lim *et al.*, 2020). Cell cycle arrest is an integral part of the DDR, providing the necessary time for repair to take place, thus ensuring the integrity of genetic material (Muschel *et al.*, 1991; Raleigh & O'Connell, 2000; Chen *et al.*, 2017). In *Arabidopsis thaliana* (hereafter Arabidopsis), cell cycle arrest in response to DNA damage occurs mostly at G2/M and G1/S phase checkpoints (De Schutter *et al.*, 2007; Cui *et al.*, 2017; Cabral *et al.*, 2020). Different

sources of DNA damage induce different types of lesions, resulting in cell cycle arrest at different cell cycle stages (Cui *et al.*, 2017; Takahashi *et al.*, 2019).

RAD51 protein plays a key role in repair via HR. RAD51 promotes essential strand-invasion step where resected 3′ single-stranded DNA end aligns with a homologous template, ensuring proper placement of broken DNA strand overhangs (Shinohara *et al.*, 1992; Li *et al.*, 2004; Abe *et al.*, 2005; Wang *et al.*, 2014; Su *et al.*, 2017; Banerjee & Roy, 2021; Yu *et al.*, 2023). The widespread presence of RAD51 homologs across various species underscores its fundamental functional significance (Bonilla *et al.*, 2020). In animals, mutations of the *RAD51* gene are lethal, but this is not the case in plants, such as Arabidopsis, in which *RAD51* is not essential for vegetative growth (Lim & Hasty, 1996; Tsuzuki *et al.*, 1996; Li *et al.*, 2004). Upon DNA damage, *RAD51* transcription is activated (Wang *et al.*, 2014; Feng *et al.*, 2017; Ryu *et al.*, 2019; Da Ines *et al.*, 2022) in a dose-dependent manner (Osakabe *et al.*, 2005; De Schutter *et al.*, 2007). RAD51 protein is subsequently loaded onto the lesion site by BRCA2 or CX3 complex (Wang *et al.*, 2010; Su *et al.*, 2017). This accumulation of RAD51 at the broken strand overhang (Flott *et al.*, 2011; Biedermann *et al.*, 2017; Da Ines *et al.*, 2022) facilitates the search for a homologous donor template (Coïc *et al.*, 2011; Hicks *et al.*, 2011; Meschichi *et al.*, 2022). The activity of RAD51 is tightly regulated at the post-translational level, serving as a substrate of multiple kinases in human (Sørensen *et al.*, 2005; Chabot *et al.*, 2019; Woo *et al.*, 2021) and budding yeasts (Flott *et al.*, 2011; Woo *et al.*, 2020, 2021). Although RAD51 phosphorylation by the cyclin kinase CDKB1–CYCB1 complex was reported *in vitro* for Arabidopsis, its exact function remains elusive. Nevertheless, it is highly likely that this process is linked to RAD51 activation and recruitment to the DNA double-strand break sites, as evidenced by compromised RAD51 foci formation in *cycb1;1* mutants (Weimer *et al.*, 2016).

Most plant studies have analyzed *RAD51* expression using bulk measurements, combining material from multiple plants (Wang *et al.*, 2014; Ryu *et al.*, 2019). Although this approach is suitable for many purposes, it does not allow determining how gene expression is tuned at the level of individual plants, tissues, or cell types. In this study, we used single-molecule RNA FISH (smFISH) (Duncan *et al.*, 2017; Zhao *et al.*, 2023) to quantify the transcriptional response of *RAD51* at the cellular level to increasing amounts of DNA damage induced by DNA damaging agent zeocin (Adachi *et al.*, 2011). Our findings show a positive correlation between *RAD51* transcription and increasing amounts of damage. Notably, *RAD51* transcriptional response differed among root cell types and developmental zones. Our data also demonstrates *RAD51* transcription outside S/G2 cell cycle phases under DNA damage, challenging the proposed strict association between HR and S/G2 phases.

Materials and Methods

Plant material

All *Arabidopsis thaliana* (L.) lines used in this study were derived from Columbia (Col-0) ecotype. Transgenic lines used in this study come from the following sources: RAD51-GFP line (Da

Ines *et al.*, 2013), Cytrap (Aki & Umeda, 2016), PlaCCI and CDT1-CFP lines (Desvoyes *et al.*, 2020).

Plant growth

Arabidopsis seeds were surface-sterilized in 5% (v/v) sodium hypochlorite for 5 min and rinsed three times in sterile distilled water. Seeds were then stratified for 2 d at 4°C before germination in a growth chamber in a vertically oriented Petri dish containing 1% plant agar (P1001.1000; Duchefa Biochemie, Haarlem, the Netherlands) MS medium plate, pH 5.7 (Gamborg *et al.*, 1976). Plants were grown under a photoperiod of 16 h day and 8 h night and a temperature cycle of 22°C during the day and 20°C during the night.

DNA damage induction

Induction of DSBs in root tissue was achieved by subjecting seedlings to overnight (12 h) exposure to zeocin (10 072 492; Gibco, Grand Island, NY, USA) on 1% plant agar MS medium plates containing the specified zeocin concentrations (10 μM, 50 μM, 170 μM).

Expression analysis using RT-PCR (real-time-qPCR)

Total *RAD51* mRNA amount was quantified in 10-d-old seedlings of Arabidopsis (Col-0) by quantitative real-time polymerase chain reaction. After zeocin exposure, the roots were excised with a razor blade and collected. A total of 0.1 g of roots per zeocin concentration was used. RNA was isolated using Qiagen RNeasy Plant Mini kit (74 904; Qiagen). RNA concentration was measured using Nanodrop ND-1000 spectrophotometer. A total of 1 μg of RNA was treated with DNase (EN0521; Thermo Fisher, Waltham, MA, USA) and reverse transcribed with Reverse Transcriptase (EP0441; Thermo Fisher). This template was then used to quantify relative mRNA abundance using the SensiMix SYBR Low-ROX kit (Bioline, London, UK), a LightCycler® 480 (Roche) and the primers described below. *RAD51* expression was analyzed using normalization to *PP2A* gene using following primers: *Rad51* forward GCGCAAGTAGATGGTTCAGC, *Rad51* reverse TTCCTCAACGCCAACCTTGT, *PP2A* forward TAACGTGGCCAAAATGATGC, and *PP2A* reverse GTTCTCCACAACCGCTTGGT. Reactions were performed in triplicate, results were calculated using the $2^{-\Delta\Delta C_t}$ method, and SD values shown on a graph. Statistical analysis was performed on a dataset containing three biological replicates.

Single-molecule fluorescence *in situ* hybridization (smFISH) on root squashes

smFISH was performed on 5–6-d-old seedlings according to previously published protocol (Duncan *et al.*, 2017) using probes designed against *RAD51* and *PP2A* genes (Supporting Information Table S1). Seedlings were collected after overnight zeocin exposure and treated further according to protocol. In brief, the experimental procedure involved preparing root tip samples of seedlings from media, fixing them in 4% paraformaldehyde, and

New Phytologist Foundation

then washing them with nuclease-free 1× PBS. Subsequently, the roots were arranged on poly-L-lysine slides, coverslipped, and squashed to expose the meristems, which were then flash-frozen in liquid nitrogen. After removing the coverslips, the roots were allowed to dry before immersing them in 70% ethanol for tissue permeabilization. Following ethanol evaporation, the samples were washed with a formamide-containing buffer. Hybridization with probe solutions was carried out overnight at 37°C, after which unbound probes were removed by washing. DAPI nuclear staining was performed. Samples were mounted in GLOX buffer and sealed for immediate imaging.

Immunodetection

Five- to six-day-old seedlings were transferred onto MS medium containing selected concentrations of zeocin overnight. Roots were then excised using a razor blade and fixed in 4% paraformaldehyde solution for 30 min in glass dishes. Subsequently, roots were washed twice with 1× PBS, arranged on a slide, covered by a glass coverslip, and squashed manually by applying pressure on coverslip. The slide was then submerged in liquid nitrogen until freezing and taken out. The coverslip was subsequently removed using a razor blade. Slides were left to dry at room temperature for 30 min. Samples were rinsed with 1× PBS three times and incubated with blocking buffer (0.5% BSA (A7030; Sigma-Aldrich) in 1× PBS) in humid chamber at 37°C for 30 min. To ensure minimal disturbance of the sample, we used small pieces of polypropylene waste bags instead of glass coverslips at all incubation stages of the protocol. Excess blocking buffer was removed, samples were incubated at 37°C overnight in a humid chamber with γH2AX primary antibody (Charbonnel *et al.*, 2010), provided by Charles White. Antibody was diluted 1 : 700 in 0.5% BSA. Slides were then rinsed with PBST buffer three times (1× PBS, 0.01% Tween20 (8.22184; Sigma-Aldrich)) and incubated with PBST buffer for 5 min. Secondary antibody (AS09633; Agrisera, Vännäs, Sweden) diluted 1 : 200 in 0.5% BSA was then applied, and samples were incubated in a humid chamber at 37°C for 2 h. Slides were rinsed three times with PBST buffer and incubated with 1× PBS buffer 2× 5 min. Excess buffer was removed, and samples were mounted in Vectashield medium (H-1000; Vector Laboratories, Peterborough, UK) containing DAPI diluted 1 : 1000 (62 248; Thermo Fisher).

Sequential smFISH and immunodetection

SmFISH and immunodetection protocols were performed sequentially in the described order. SmFISH in root squashes was performed first according to the referred protocol (Duncan *et al.*, 2017). After imaging, the coverslips were gently removed using additional volumes of 1× PBS. Samples were rinsed with 1× PBS three times, and samples were processed according to immunodetection protocol above.

Whole-mount smFISH (WM-smFISH)

WM-smFISH was performed on 5–6-d-old seedlings according to previously published protocol (Zhao *et al.*, 2023) using probes

designed against *RAD51* gene (Table S1). In brief, roots were immersed in a small glass dish containing 4% paraformaldehyde and left to incubate for 30 min at room temperature. Subsequently, they underwent two washes with 1XPBS and were then treated with 100% methanol for two 15-min intervals, followed by two similar treatments with 100% ethanol. Tissue clearing was achieved by exposing the samples to ClearSee at 4°C in the dark overnight. Afterward, the roots were washed twice with Stellaris wash buffer A (Cat. #SMF-WA1-60; LGC Biosearch Technologies, Hoddesdon, UK) for 15 min each. Samples were then carefully arranged on a poly-L slide, ensuring excess wash buffer was removed without allowing the samples to dry. To each slide, 20 µl of activated embedding solution was added before covering them with a coverslip. Polymerization was allowed to occur at room temperature for a minimum of 20 min before carefully removing the coverslip.

For probe hybridization, a hybridization solution was prepared by combining 0.5 µl of each required probe set stock solution with 100 µl of hybridization buffer (containing 10% dextran sulfate, 2 × SSC, and 10% formamide) to achieve a final concentration of 250 nM. One hundred microliters of this hybridization solution was applied to each slide, covered with a coverslip to prevent evaporation, and placed in a humid chamber at 37°C overnight in the dark.

Subsequently, the coverslip was removed, and the slides were submerged twice in 50 ml of wash buffer (containing 10% formamide and 2 × SSC) for 30 min each in an opaque coplin jar. Once removed from the coplin jar, the samples were stained at 37°C for 10 min in the dark by adding 100 µl of the desired dye solutions (such as DAPI or SCRI Renaissance 2200) to each slide. After staining, excess buffer was removed, and each slide was mounted with 20 µl of vectashield (Cat.# H-1000-10; Bio-Nordika, Stockholm, Sweden). Covering the samples with a coverslip, excess vectashield was removed, and they were sealed with nail varnish. To prevent fluorophore fading, imaging of the slides was conducted on the same day.

Sequential WM-smFISH and 5-ethynyl-2′-deoxyuridine (EdU) labeling

Five- to six-day-old seedling were first transferred onto the MS medium containing zeocin for 10 h. Seedlings were then transferred onto MS medium containing same concentration of zeocin and 20 µM EdU (A10044; Invitrogen) for 2 h. WM-smFISH was performed first according to the described protocol. After imaging, coverslips were gently removed from the samples using additional volumes of 2× SSC buffer. Samples were then rinsed with 2× SSC buffer three times and incubated with 3% BSA in 1× PBS solution at 37°C in a humid chamber for 15 min. Samples were incubated with Click-iT reaction cocktail (C10269; Invitrogen) mixed according to the manufacturer's instructions with addition of Alexa Fluor 488 azide (A10266; Thermo Fisher), 500× dilution. Samples were then rinsed and incubated with a wash buffer (10% formamide (17899; Thermo Scientific) and 2xSSC) for 5 min. Samples were incubated with SCRI Renaissance 2200 solution (Musielak *et al.*, 2015) for 15 min at 37°C in a humid chamber. Slides were rinsed and incubated for

5 min in the wash buffer. Samples were then mounted in a drop of Vectashield medium.

RAD51 mRNA half-life quantification

Five- to six-day-old seedling were transferred onto MS medium containing 10 µM zeocin for selected time periods: 12, 10, 8, 6 h. Seedlings exposed to zeocin for 10, 8, and 6 h were then transferred to MS medium containing 10 µM zeocin with actinomycin D (J60148.LB0; Thermo Fisher) or 10 µM zeocin with DMSO (D4540; Sigma-Aldrich) for 2, 4 and 6 h accordingly. Seedlings were then collected and processed according to smFISH protocol for root squashes using probes for *RAD51* gene. The decay rate (k_{decay}) for *RAD51* and then its half-life ($t_{1/2}$) were calculated by adjusting the number of molecules per cell (n) counted in the smFISH images as an exponential function of time (t). The mathematical adjustment for $n(t)$ was developed in R assuming a constant decay rate, according to the function: $n(t) = e^{-k_{decay} \times t}$, then the half-life was calculated using the formula: $\log_e (2)/(k_{decay})$ (Narsai *et al.*, 2007; Sorenson *et al.*, 2018).

DAPI intensity measurements

DAPI signal intensity was evaluated in whole-mounted roots of the Cytrap line processed according to WM-smFISH protocol but without smFISH detection. Roots embedded in polyacrylamide gel were mounted in Vectasield containing DAPI diluted 1 : 1000. Samples were imaged on a confocal microscope choosing the median plane of the root. ImageJ software was used to determine total integrated density of DAPI-stained nuclei. S/G2 and G2/M cells were identified by expression of the corresponding marker, and predicted G1 (pG1) cells were identified by absence of a marker.

Image acquisition

Samples were imaged on Zeiss LSM780 and LSM800 inverted confocal microscopes (Zen Black Software) using a 63× water-immersion objective (1.20 NA). smFISH on root squashes imaging was performed using widefield mode, and we used a cooled quad-port charge-coupled device ZEISS Axiocam 503 mono camera. A series of optical sections with z-steps of 0.22 µm were collected throughout the whole cell volume. For DAPI imaging, an excitation filter of 335–383 nm was used, and emission was collected at 420–470 nm. smFISH probes labeled with Quasar570 were imaged using 533–558 nm excitation filter and 570–640 nm signal detection range. Immunostaining experiments were imaged in confocal mode. DAPI signals were imaged using 405 nm excitation line with emission detection at 410–600 nm. Secondary antibody (AS09633; Agrisera) signal was imaged with 488 nm excitation line and emission detection at 490–540 nm. Imaging was performed in a manually adjusted single plain selected to have a maximal number of nuclei in focus.

WM-smFISH imaging was performed in confocal mode using a 63× water-immersion objective (1.20 NA). For SCRI Renaissance 2200 imaging, we used a 405 nm laser line, and emission was collected at 400–560 nm. smFISH probe signals were captured with 561 nm excitation line and emission collected at 535–617 nm.

PlaCCI reporter line CFP, YFP, and RFP signals were imaged with 458 nm, 514 nm, and 561 nm excitation lines and emission detection at 456–563 nm, 518–598 nm, and 580–696 nm, respectively. Cytrap reporter line GFP and RFP signals were imaged with 488 nm and 561 nm excitation lines and emission detection at 490–560 nm and 562–700 nm accordingly.

Image analysis

smFISH Nuclei and cellular outlines in smFISH were defined using the CellProfiler software (Stirling *et al.*, 2021). RNA foci were detected and counted using FISH-quant-v.3 (Mueller *et al.*, 2013) in Matlab. First, the 'cell segmentation' tool was used to generate text files with the outline coordinates for the nuclei and cell masks. The outlines were uploaded, and images were pre-processed for increasing their signal-to-noise ratio though a dual-Gaussian filtering followed by a Gaussian Kernel. Dots were detected in the filtered image, first pre-detecting fluorescent foci with fluorescence over a threshold. Then, the pre-detected dots were fitted to a Gaussian fluorescence based on a point-spread function. Images were analyzed in the batch mode, and false positives were removed in the end by thresholding the Sigma-XY, amplitude, and pixel-intensity parameters to Gaussian distributions.

WM-smFISH Cell segmentation was performed with the Cellpose software (Stringer *et al.*, 2021), using an algorithm trained by us. RNA foci were detected and counted using FISH-quant-v3 (Mueller *et al.*, 2013) as described above. For RAD51-GFP line, the signal intensities of both mRNA and protein channels were quantified in the CellProfiler software (Stirling *et al.*, 2021). Colocalization analysis and heatmap visualization were performed using the CellProfiler software (Stirling *et al.*, 2021).

Cell cycle evaluation from images of EdU staining, Cytrap, and PlaCCI lines was performed manually using the ImageJ software.

Correlation analysis of ɣH2AX signal and *RAD51* transcription Data on *RAD51* transcription and ɣH2AX levels were collected from the same cells for correlation analysis. ɣH2AX integrated density was measured using the ImageJ software and normalized to DAPI integrated density. The number of detected *RAD51* mRNA molecules was normalized by the cell area to correct for cell size difference. Values obtained for both parameters were log-transformed. Data were visualized, and correlation was evaluated using R studio ggplot2 package.

Results

RAD51 transcriptional response to increasing DNA damage levels

To elucidate *RAD51* transcriptional response to DNA damage, we first assessed *RAD51* mRNA levels on roots from Arabidopsis plants treated with increasing concentrations of the DSB-inducing agent zeocin (0 µM, 10 µM, 50 µM, 170 µM) using real-time
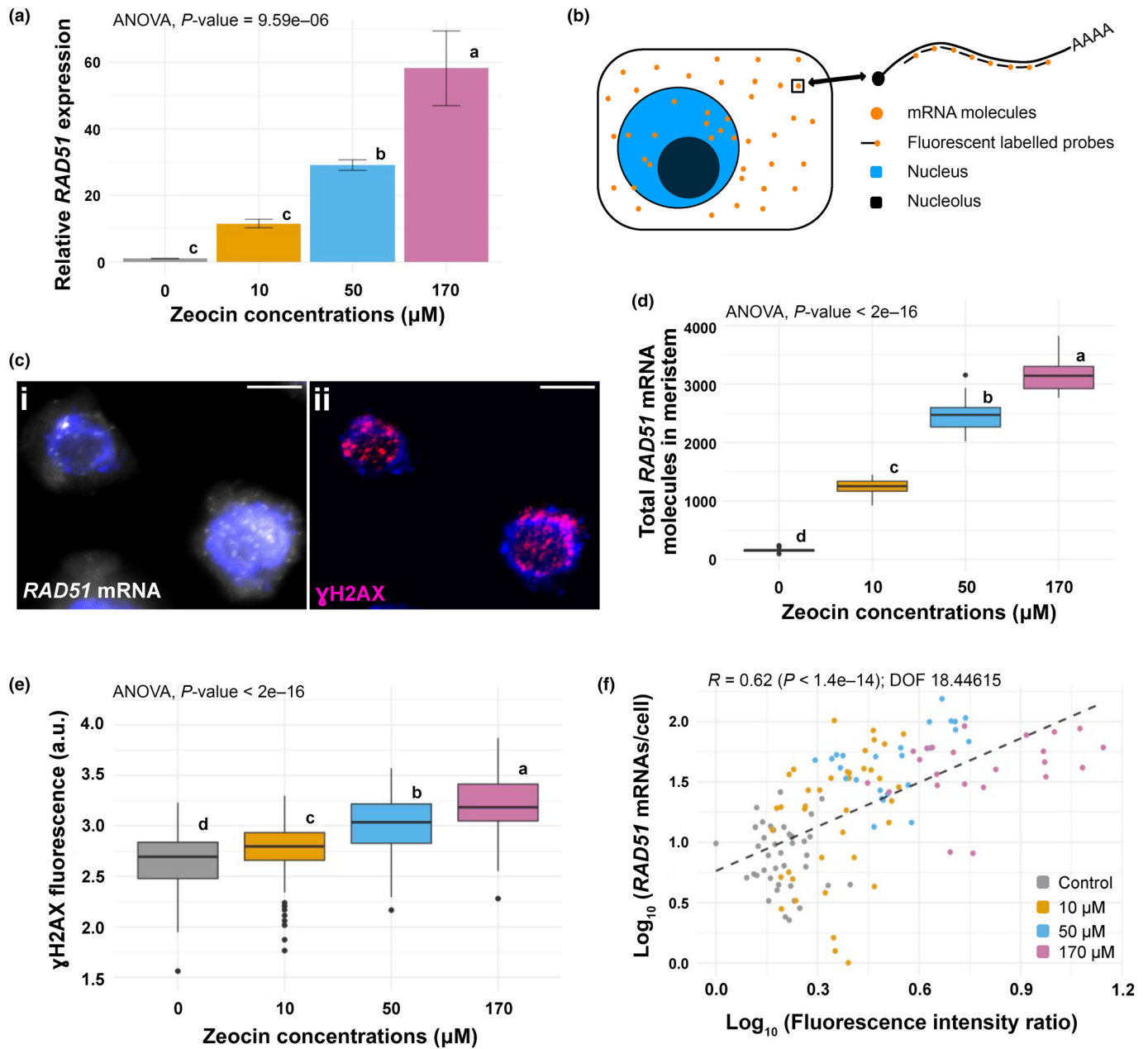
Fig. 1 *RAD51* transcript and γH2AX levels in Arabidopsis root squashes under increasing DNA damage. (a) Expression analysis of *RAD51* mRNA by qPCR, after exposure to different concentrations of zeocin. *RAD51* expression measured relative to *PP2A* gene. (b) Schematic image of single-molecule mRNA detection by single-molecule RNA FISH protocol. (c) Representative images of sequential smFISH/Imunofluorescence protocol, for a 50 μM zeocin treatment. (i) *RAD51* mRNA signals (white), nuclei counterstained with DAPI (blue). (ii) γH2AX immunodetection (magenta) and DAPI (blue). Bars: 5 μm. (d) Total number of *RAD51* mRNA molecules detected in root meristems. A subset of 30 meristematic cells was randomly chosen from the initial dataset, consisting of $n = 160$; 116; 60, 96 cells (for 0 μM, 10 μM, 50 μM, and 170 μM zeocin, respectively). Quantification was performed by counting the total number of *RAD51* mRNAs within the 30 sampled cells. This process was iterated 30 times to produce the box plots. (e) Quantitative analysis of immunofluorescence experiment using anti-γH2AX antibody. Values represent fluorescence intensity measured as integrated densities in arbitrary units ($n = 236$, $n = 145$, $n = 226$, $n = 182$ cells for 0 μM, 10 μM, 50 μM, 170 μM zeocin, respectively). (f) Correlation analysis between the number of *RAD51* mRNAs and γH2AX signal intensity in individual cells with linear model fit. Number of *RAD51* mRNA molecules was normalized by corresponding cell area. γH2AX fluorescence intensity measured as integrated density with prior normalization to DAPI signal. Correlation coefficient (R) and P-value are shown on the graph. Deviance of fit indicates deviance of fit calculated for the model. Dataset contains $n = 40$, $n = 40$, $n = 25$, $n = 22$ measurements for 0 μM, 10 μM, 50 μM, 170 μM zeocin, respectively. Throughout this figure, significance tested by ANOVA (P-values are shown on the graph). Letters indicate results of Tukey's HSD test with 95% confidence level. Error bars indicate SD. Boxplots demonstrate median value (horizontal line), first and third quartile (colored rectangle), 1.5× interquartile range (whiskers), and outliers (black points).

quantitative polymerase chain reaction. The results demonstrated an increase in *RAD51* mRNA levels with increasing zeocin concentrations (Fig. 1a). To investigate *RAD51* transcriptional upregulation as a function of DNA damage at the cellular and tissue level, we employed smFISH (Duncan *et al.*, 2016). SmFISH uses a set of oligo probes (each 18–22 nt long), directly labeled with a fluorophore and designed to tile along a specific RNA of interest (Fig. 1b). This method detects fluorescent dots corresponding to single mRNA molecules, which can be automatically detected and counted to provide absolute counts of mRNA molecules per cell (Raj *et al.*, 2008; Duncan *et al.*, 2016). The results of smFISH experiment on Arabidopsis root squashes revealed an increase in the total number of *RAD51* transcripts in the root meristem with increasing zeocin concentrations, consistently with qPCR data (Fig. 1d). To assess the increase in DNA damage levels corresponding to increasing zeocin concentrations, we quantified γH2AX levels by immunodetection as a proxy marker for DSB levels in individual root cells. Single-cell layers achieved by root squashing facilitated antibody penetration required for immunodetection (Fig. 1c(ii)). The results showed an increase of γH2AX levels in response to increasing zeocin concentrations (Fig. 1e), indicating a rise in the number of DSBs per cell. Of note, both the increase in γH2AX accumulation and the number of *RAD51* mRNAs were not directly proportional to the increase in zeocin concentration. To investigate the direct relationship between the number of *RAD51* mRNAs and the extent of DNA damage within individual cells, we performed a sequential *RAD51*-smFISH/γH2AX-immunodetection protocol on cells obtained from root squashes and evaluated the number of mRNAs and DNA damage levels on the same cells (Fig. 1c). This analysis revealed a positive correlation between the number of *RAD51* mRNA molecules per cell and the γH2AX levels with a correlation coefficient $R = 0.62$ ($P < 1.4e^{-14}$) (Fig. 1f). Our analysis indicated that the interaction between the two variables is best described by a linear model with deviance of fit (DOF) value of 18.44615. Interestingly, the DOF value of the exponential model, which suggests a potential limit to the number of *RAD51* mRNAs per cell, was only slightly higher, 18.99684 (Fig. S1a). To gain a better insight into *RAD51* transcriptional response to increasing DNA damage, we quantified *RAD51* transcription sites after exposure to different concentrations of zeocin. Assessing the signal intensity of transcription sites (visible as brighter foci in the nucleus) relative to the mean single mRNA intensity allows us to estimate the number of nascent RNAs. Analysis of the transcription sites revealed an increase in *RAD51* nascent signals with higher zeocin concentrations (Fig. S2a), thus supporting the linear model (Fig. 1f). Importantly, the mRNA counts for the house-keeping gene *PP2A* using smFISH method revealed that the number of *PP2A* mRNAs/cell remained constant across zeocin concentrations (Fig. S1b), validating the specific *RAD51* mRNA accumulation with increasing damage.

Cell-to-cell variability in *RAD51* transcriptional response

The recently developed WM-smFISH method overcomes the limitations of traditional root squash sample preparation, enabling the assessment of transcript numbers within intact tissues and comparison between cell types and developmental zones of the root (Fig. 2a) (Zhao *et al.*, 2023). Heatmaps of *RAD51* were generated to visualize the number of mRNAs per cell across root tissues (Figs 2b, S3). The results revealed that the number of transcribing cells as well as the number of *RAD51* mRNA molecules detected per cell increases in response to increasing zeocin concentrations. This pattern is evident in the histogram quantification (Fig. S2b), depicting a progressive rise in the number of transcribing cells with increasing zeocin concentrations. To demonstrate the accuracy of *RAD51* mRNA quantification, we present close-up images of cells with varying counts (Fig. S4). Importantly, our results indicate substantial variability among root cells in their sensitivity to DSBs induced by zeocin, as revealed by the non-uniform heatmaps (Figs 2, S3). Some cells exhibited a strong transcriptional response even at a 10 μM zeocin concentration, with mRNA counts comparable to those induced by 50 μM and 170 μM (Fig. 2b). Conversely, certain cells displayed low mRNA counts even after exposure to 50 μM and 170 μM zeocin (Fig. 2b). To discern potential distinctions between cell types, we plotted the number of *RAD51* mRNAs in different root cell types (Epidermis, Cortex, Endodermis, and Stele) (Fig. 2c,d). The results demonstrated that *RAD51* transcriptional response within stele cells was distinct from the other root cell types analyzed showing higher per cell mRNA counts (Fig. 2d). Two-way ANOVA analysis showed significant ($P = 0.038$) interaction between zeocin concentration and cell type parameters (Fig. 2d). Using data from multiple roots, we also compared the number of *RAD51* mRNAs between stem cells and root meristem cells, subjected to increasing zeocin concentrations (Fig. S5). Meristematic cells exhibited the reported increasing trend of *RAD51* mRNAs, while in stem cells, the highest levels were observed following a 10 μM zeocin treatment. This observation is likely attributed to the previously reported stem cell death with high zeocin concentrations (Fulcher & Sablowski, 2009). Indeed, post-damage recovery assessment showed that seedlings exposed to 10 μM zeocin recovered main root growth, whereas recovery in plants exposed to 50 μM and 170 μM zeocin was delayed and required lateral root formation (Fig. S6). Across developmental regions, *RAD51* transcriptional output exhibited a decrease in the elongation zone compared with the meristem region (Fig. S7), consistent with previous reports (Da Ines *et al.*, 2013).

Quantification of RAD51 protein levels per cell

To investigate the relationship between *RAD51* mRNA and protein levels per cell, we performed WM-smFISH on RAD51-GFP line (Da Ines *et al.*, 2013) (Fig. 3a). RAD51-GFP line carries a transformed in-frame translational fusion reporter transcribed from the endogenous promoter of *RAD51* gene in *rad51/rad51* background. The resulting protein construct shows partial functionality such as assembly at the DSB sites, while its DSB repair function is compromised (Da Ines *et al.*, 2013). Performing WM-smFISH on this line enables simultaneous detection of *RAD51-GFP* mRNA and RAD51-GFP protein levels in the same cells. Similarly to Col-0 plants, *RAD51-GFP* mRNA levels per cell increased with increasing zeocin concentration (Fig. 3a(ii,iv), b), and a similar trend was observed for RAD51-GFP protein
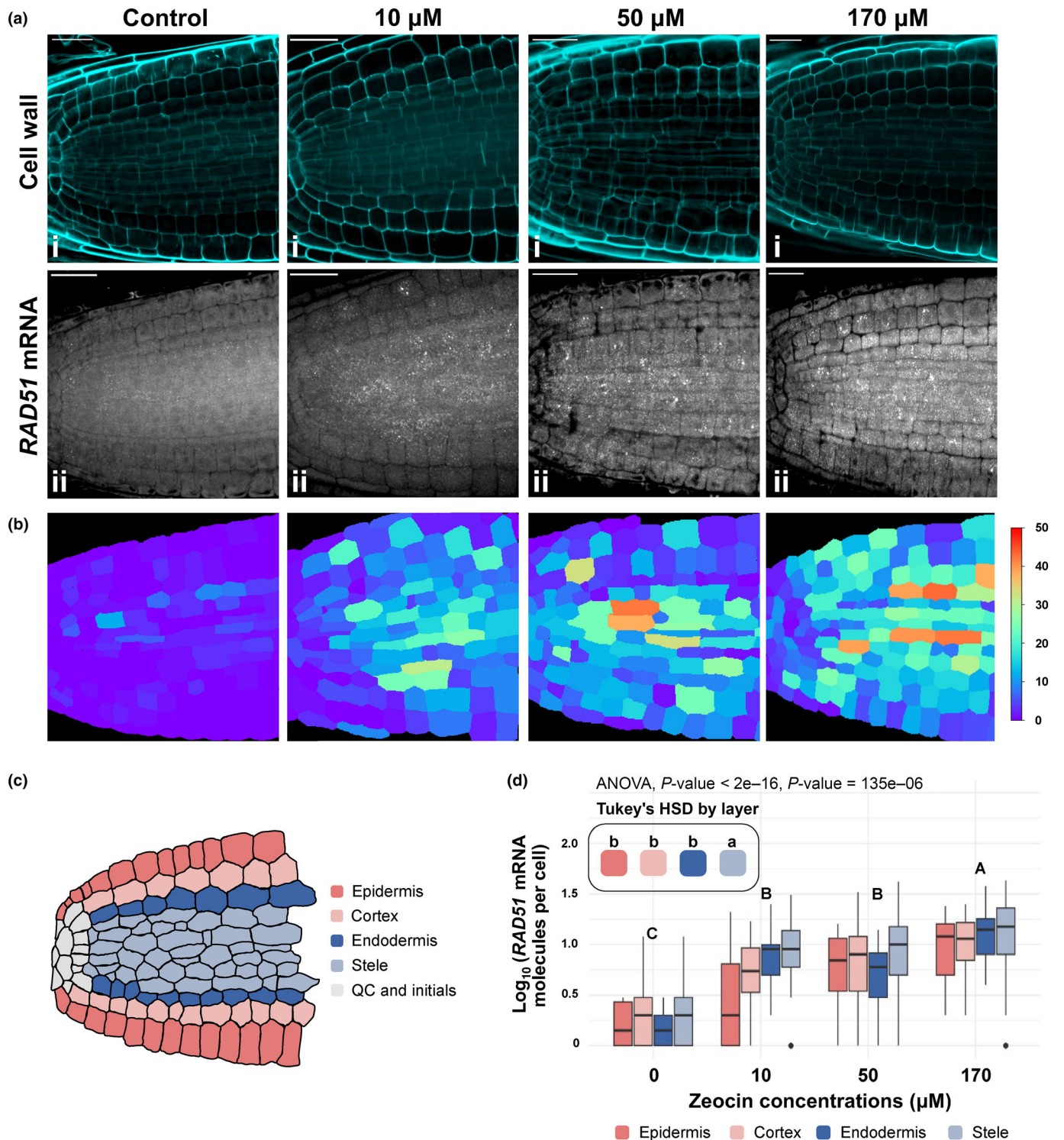
Fig. 2 *RAD51* mRNA transcriptional response in different cell types of Arabidopsis root. (a) Representative images of whole-mount single-molecule RNA fluorescence *in situ* hybridization for *RAD51* mRNA in Col-0 roots after exposure to 0 μM, 10 μM, 50 μM, 170 μM concentrations of zeocin. (i) Images of cell wall staining using Renaissance 2200 dye. (ii) Images of *RAD51* mRNA detection. Bars: 20 μm. (b) Heatmaps showing quantification of *RAD51* mRNA molecules detected in individual cells. (c) Schematic representation of the Arabidopsis root tip and its cell types. (d) Number of *RAD51* mRNA molecules per cell in each of the selected cell types (Epidermis, Cortex, Endodermis, Stele) after exposure to different concentrations of zeocin. Two-way ANOVA revealed statistically significant difference in *RAD51* molecule number by both zeocin concentration ($P = 2e-16$ (and cell type) $P = 1.35e-06$). Letters indicate results of Tukey's HSD test of two-way ANOVA results with 95% confidence level. Boxplots demonstrate median value (horizontal line), first and third quartile (colored rectangle), 1.5× interquartile range (whiskers), and outliers (black points). Measurements for (d) performed using data from images (a, b).
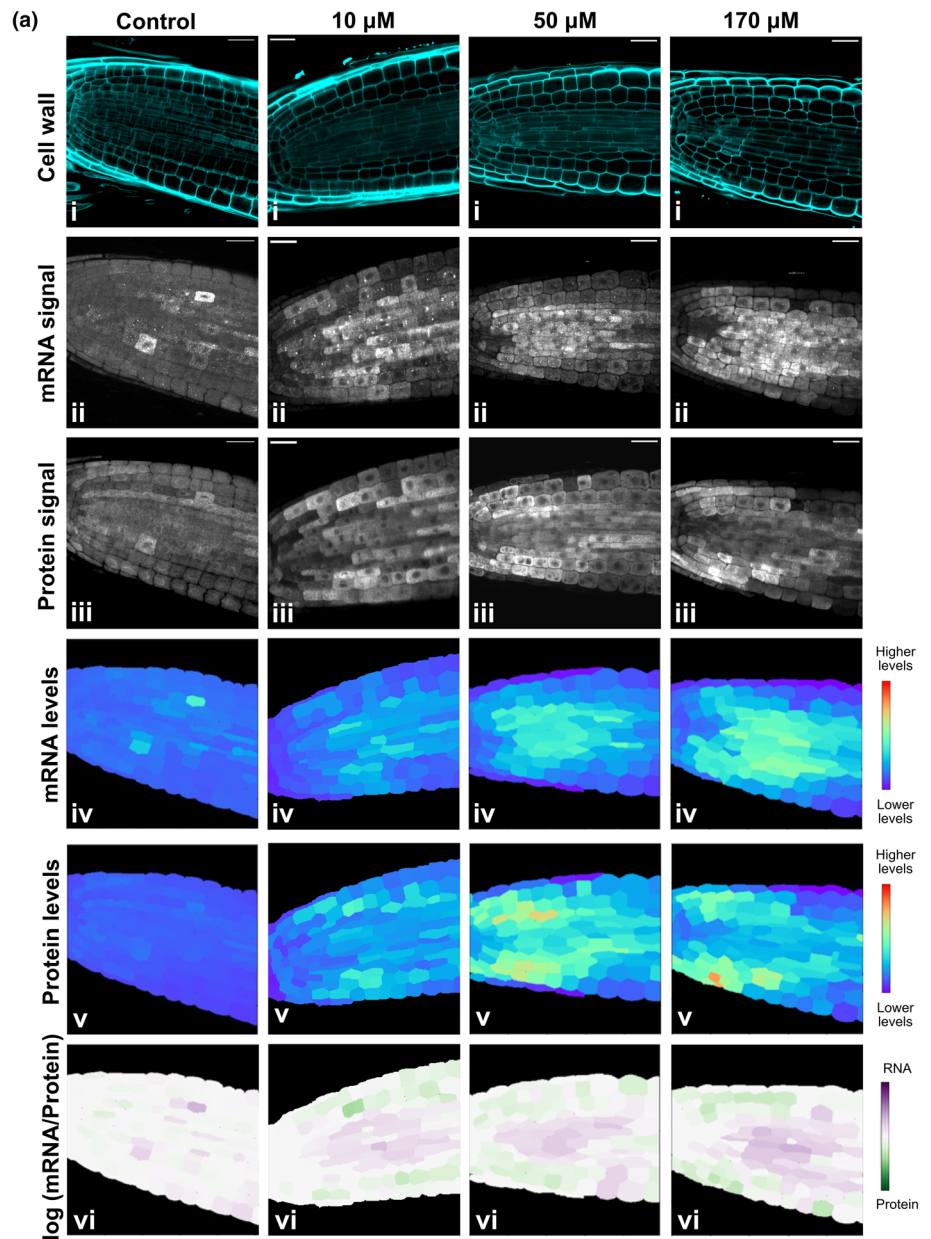
Fig. 3 Simultaneous detection and quantification of *RAD51-GFP* mRNA and protein in response to increasing DNA damage. (a) Representative confocal images and quantification heatmaps of *RAD51-GFP* mRNA (ii) and RAD51-GFP protein signals (iii) after exposure to 0 µM, 10 µM, 50 µM, 170 µM concentrations of zeocin. (i) Images of cell wall staining using Renaissance 2200 dye. Images of *RAD51-GFP* mRNA obtained using whole-mount single-molecule RNA fluorescence *in situ* hybridization and (ii) RAD51-GFP fluorescent protein signals (iii). (iv, v) Heatmaps representing the levels of the corresponding mean mRNA signal intensity per cell (iv) and mean protein signal intensity per cell (v). (vi) Heatmaps representing the ratio between the *RAD51-GFP* mRNA and RAD51-GFP protein signal intensities in each cell. Bars: 20 µm. (b) Quantification of *RAD51-GFP* mRNA mean signal intensity per cell for the different zeocin treatments. (c) Quantification of RAD51-GFP protein mean signal intensity per cell for the different zeocin treatments. Graphs on (b, c) created using dataset from several images ($n = 640$, $n = 1391$, $n = 854$, $n = 457$ cells for 0 µM, 10 µM, 50 µM, 170 µM zeocin respectively). Significance tested by ANOVA (*P*-values are shown on the graph). Letters indicate results of Tukey's HSD test with 95% confidence level. Error bars indicate SD. Boxplots demonstrate median value (horizontal line), first and third quartile (colored rectangle), 1.5× interquartile range (whiskers), and outliers (black points).

(Fig. 3a(iii,v),c). Intriguingly, heatmaps evaluating ratio between mRNA and protein levels revealed differences between cells in terms of mRNA and protein accumulation (Figs 3a(vi), S8–S10). In line with our previous observations, mRNA molecules seem to have a higher abundance in stele (Figs 3a(ii,iv,vi), S8–S10). RAD51-GFP protein accumulation, on the other hand, was more prevalent in the cortex and epidermis of the root tip (Figs 3a(iii, v,vi), S8–S10). This differential accumulation between mRNA and protein among different cell types is intriguing and could suggest differences in mRNA translation efficiency, protein movement, or differential degradation between cells but more investigation to validate these hypotheses would be required.

RAD51 transcription through the cell cycle

RAD51 transcription is typically linked to the S and G2 phases of the cell cycle, motivated by the requirement of homologous DNA sequences during repair through HR (Schuermann *et al.*, 2005; Goldfarb & Lichten, 2010). Given the very high proportion of cells with *RAD51* mRNAs signals in zeocin-treated samples, we expected a considerable number of cells arrested at the S or G2/M checkpoints (Osakabe *et al.*, 2005; De Schutter *et al.*, 2007). To evaluate the cell cycle arrest in roots treated with zeocin, we conducted EdU staining to label cells that went through S phase using a sequential smFISH/EdU protocol
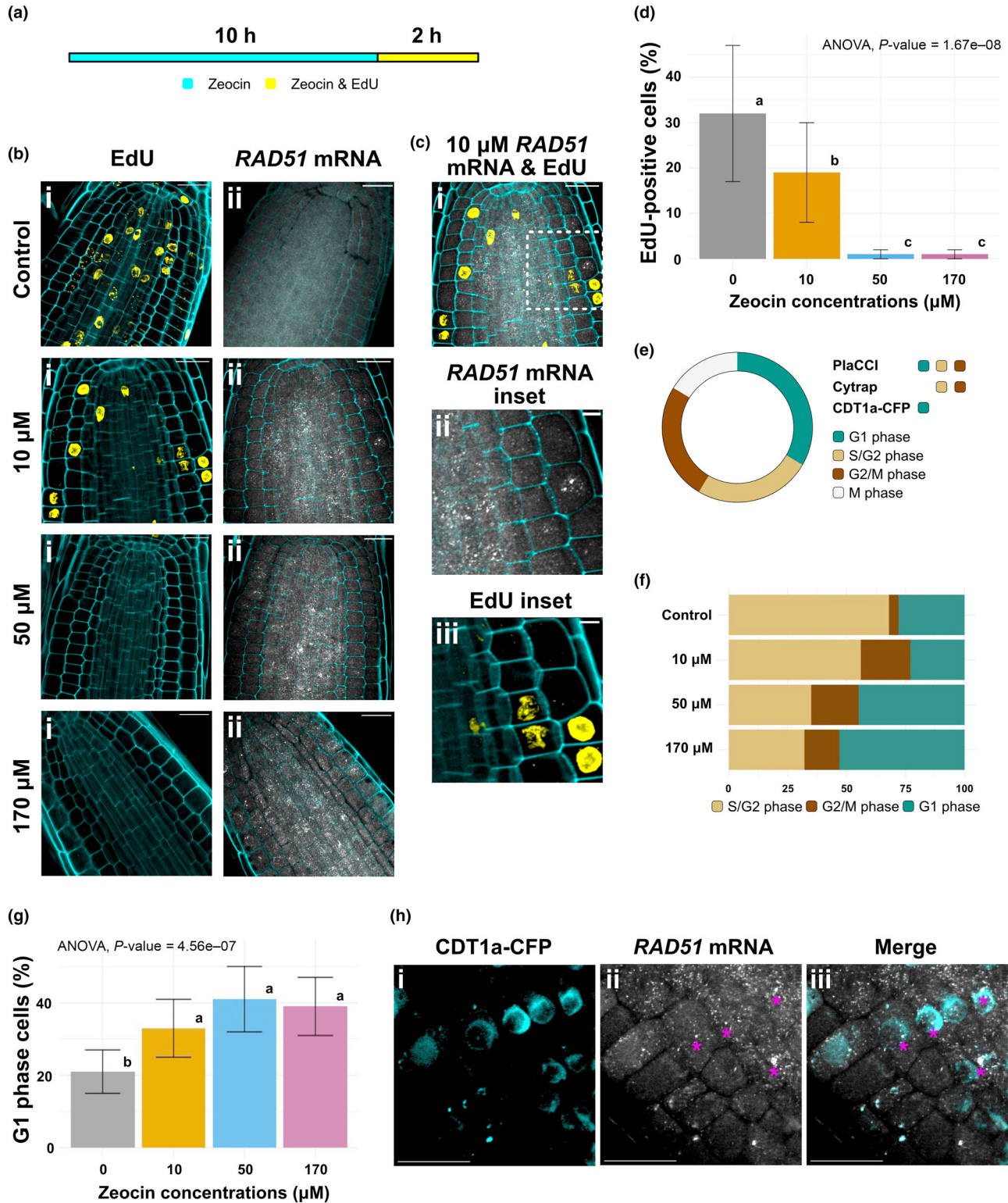
Fig. 4 Dynamics of *RAD51* transcription throughout the cell cycle in response to DNA damage. (a) Scheme of experimental setup used for quantification of S phase cells. Seedlings were treated with different concentrations of zeocin concentrations for 10 h, followed by an additional treatment with zeocin and 5-ethynyl-2′-deoxyuridine (EdU) for 2 h. (b) Confocal images of roots acquired using sequential WM-smFISH/EdU protocol after exposure to different zeocin concentrations. (i) Detection of S phase cells by EdU staining (yellow). (ii) *RAD51* mRNA detection by smFISH. Cell wall staining using Renaissance 2200 dye (cyan). Bars: 20 μm. (c) Images of *RAD51* mRNA and EdU staining for 10 μM zeocin with higher magnification, showing *RAD51* transcription sites in EdU-negative cells. (i) Merged image showing *RAD51* mRNA and EdU signals. White dashed box delineates magnified area. Bars: 20 μm. (ii) Magnified area showing *RAD51* mRNA signals. Bar, 5 μm. (iii) Magnified area showing EdU signals. Bar, 5 μm. (d) Percentage of EdU-positive cells in roots after exposure to zeocin ($n = 1123$, $n = 1356$, $n = 1519$, $n = 1208$ measurements for 0 μM, 10 μM, 50 μM, 170 μM zeocin, respectively). Significance tested by ANOVA (*P*-values are shown on the graph). Letters indicate results of Tukey's HSD test with 95% confidence level. Error bars indicate SD. (e) Schematic representation of the cell cycle. Phases of the cell cycle indicated by the different cell cycle reporter lines. (f) Quantification of the proportion (in percentage) of cells in different phases of the cell cycle using the Cytrap line ($n = 1002$, $n = 816$, $n = 800$, $n = 998$ individual measurements for 0 μM, 50 μM and 170 μM zeocin, respectively). (g) Percentage of G1 phase cells in roots after exposure to different concentrations of zeocin using PlaCCI line ($n = 2526$, $n = 2438$, $n = 1997$, $n = 1698$ measurements for 0 μM, 10 μM, 50 μM, 170 μM zeocin, respectively). Significance tested by ANOVA (*P*-values are shown on the graph). Letters indicate results of Tukey's HSD test with 95% confidence level. Error bars indicate SD. (h) Representative confocal image of root cells from CDT1a-CFP line after exposure to 50 μM zeocin, showing with *RAD51* mRNA signal detection via WM-smFISH. (i) Detection of CDT1a-CFP reporter. (ii) Detection *RAD51* mRNA signals. Asterisks indicate transcription sites. (iii) Overlay of (i, ii) images. Bars: 20 μm.

(Fig. 4a–c). EdU is a thymidine analogue that is incorporated into DNA during replication and can be visualized by a reaction with fluorescent azide (Salic & Mitchison, 2008). Our results revealed a drastic decline in the number of EdU-positive cells with increasing zeocin concentration, with almost no labeled cells at 50 μM and 170 μM concentrations (Figs 4b,d, S11a(i)). This indicates a strong cell cycle arrest in these samples. EdU-positive cells tend to be most abundant in the root stele (Fig. 4b), possibly explaining higher *RAD51* transcript output in these cells. Moreover, two-way ANOVA revealed that the observed variations in EdU-positive cell numbers can be explained by both zeocin concentration and the cell type with significant interaction between the two parameters ($P = 4.94e^{-15}$) (Fig. S11b). Subsequent pairwise comparisons revealed statistically significant changes in EdU-positive cells between concentrations, specifically within the root stele. Importantly, comparing EdU labeling with *RAD51* smFISH signals revealed cells with no EdU signal and abundant number of *RAD51* mRNA molecules (Fig. 4c). It is also noteworthy that EdU signals were observed in the root elongation zone at zeocin concentrations of 50 μM and 170 μM zeocin, indicating distinct responses across the various root developmental zones (Fig. S11a(ii)).

To further investigate the association between *RAD51* transcription and the cell cycle under DNA damage, we used Cytrap (Yin *et al.*, 2014), CDT1-CFP (Desvoyes *et al.*, 2019), and PlaCCI (Desvoyes *et al.*, 2020) lines. Cytrap line allows visualization of S to early G2 phase cells (S/G2) and late G2 to mid-M (G2/M) cells, while PlaCCI line provides the additional possibility of directly visualizing G1 phase cells using the CDT1a-CFP, a marker which is also available as a separate line (Fig. 4e). Analysis of Cytrap line revealed a decrease in S/G2 phase cells with increasing concentrations of zeocin, consistent with EdU staining data (Fig. S12a), as well as an increase in the fraction of cells expressing G2/M reporter, potentially corresponding to checkpoint arrest (Fig. S12b) (Preuss & Britt, 2003). Statistical analysis revealed that the changes in S/G2 and G2/M phase cells can be explained by both zeocin concentration and the cell type with significant interaction between the two parameters ($P = 1.08e^{-09}$, $P = 6.56e^{-06}$ accordingly) (Fig. S12e,f). Further pairwise comparisons revealed statistically significant changes between the

concentrations only for the stele, a pattern similar to the earlier reported *RAD51* transcriptional data. Importantly, at higher concentrations of zeocin, the combined percentage of S/G2 and G2/M cells suggests that a large fraction of cells could potentially be in G1 phase (Fig. 4f). Comparison of DAPI signal intensities among cells predicted to reside in different phases of the cell cycle revealed significant differences, consistent with expected variations in DNA content linked to cell cycle progression (Fig. S13a), thus reinforcing the validity of G1 phase predictions. Based on these findings, we decided to visualize cells directly in G1 phase using recently developed PlaCCI and CDT1-CFP lines. The results confirmed an increase in the amount of G1 cells in response to increasing concentrations of zeocin in these lines indicating potential cell cycle arrest at G1/S checkpoint (Figs 4g, S14a). The proportion of cells with G2/M marker also increased confirming the results obtained with Cytrap line (Fig. S14b,c). Two-way ANOVA analysis of cell cycle phase arrest in response to DNA damage in PlaCCI line revealed that the changes in G1 proportion can be explained by both zeocin concentration and the cell type with significant interaction between the two parameters ($P = 0.0268$) (Fig. S14a,d). Further pairwise comparisons revealed statistically significant increase in G1 cells only within the root stele. Intriguingly, we also observed a small fraction of cells without any fluorescent reporter presence in roots of PlaCCI line (Fig. S14c). Given that certain cell cycle markers, notably *CYCB1;1* (Weimer *et al.*, 2016), have been demonstrated to respond to DNA damage, we also adopted a cell marker-independent approach to confirm our results (Fig. S13b). Since DNA content increases during S phase, we measured the fluorescence intensity of DAPI-stained nuclei to estimate cell cycle progression. The results indicate that zeocin-exposed samples exhibited a left-skewed distribution of DAPI intensities, possibly indicating an accumulation of cells in G1, thereby supporting the results obtained with cell cycle markers.

One possible explanation for the presence of *RAD51* mRNAs in G1 cells is that these transcripts could be produced in S/G2 and carried over to G1 phase due to a potentially long half-life of RAD51 mRNAs. To evaluate *RAD51* mRNA half-life, we treated seedlings with the transcription elongation inhibitor, actinomycin D (ActD), and conducted a time-series smFISH

analysis (Fig. S15). The half-life of the *RAD51* mRNA was calculated from our data as 4.9 h. Considering this measurement, there is the possibility of *RAD51* mRNA persisting beyond the G2 phase of the cell cycle. Indeed, we detected mitotic cells, in which gene transcription normally stops, containing *RAD51* mRNAs (Fig. S15c). However, this half-life (4.9 h) is relatively short compared with the cell cycle duration (Rahni & Birnbaum, 2019), so while *RAD51* mRNA may be carried between cell divisions, its half-life alone seems unlikely to explain the high proportion of G1 cells with *RAD51* mRNA signals in zeocin samples.

To show *RAD51* transcription in G1 arrested cells directly, we performed *RAD51* smFISH detection on CDT1-CFP line (G1 marker) (Fig. 4h). The results clearly show the presence of multiple *RAD51* mRNAs and, most importantly, active transcription sites in CDT1-positive cells. Transcription sites are visible as brighter smFISH foci in the nucleus (Fig. 4h(ii)), directly confirming the predicted transcription of *RAD51* during G1 phase under DNA damage. Intriguingly, cases of G1 *RAD51* transcription were detected even in control samples (not treated with zeocin). Further examination of transcription site numbers in G1 and non-G1 cells using the CDT1-CFP line (Table S2), and analysis of *RAD51* mRNAs in EdU-positive vs EdU-negative cells (Fig. S16), suggests that *RAD51* transcription occurs with approximately equal probability in the different stages of the cell cycle.

Discussion

This study describes the transcriptional activation of *RAD51* following increasing amounts of DNA damage. Our findings indicate a rise in total *RAD51* mRNA production that results from an increase in transcriptional output per cell as DNA damage increases. These results underscore the cell's capacity to sense the extent of damage and modulate *RAD51* transcription accordingly. Using single-cell measurements by smFISH technique, we obtained data showing differences in DNA damage sensitivity between cells, manifested by varying *RAD51* mRNA transcriptional output in response to the same concentration of DNA damaging agent. Possible explanations for these observations include differences in DNA damage sensitivity, differences in *RAD51* promoter activity, or variations in the abundance of *cis*-regulators among cell types. Further studies would be necessary to pinpoint the mechanisms underlying these differences.

Cell cycle arrest and upregulation of DDR genes are the two key elements of the DDR response. Our data from several independent experiments showed that root stele cells consistently differed from the other cell types in both cell cycle changes and *RAD51* transcriptional response to increasing amounts of DNA damage. Specifically, root stele cells exhibited a more extensive *RAD51* transcriptional activation as well as larger fluctuations in numbers of cells represented at different cell cycle stages under the same zeocin concentrations. One potential explanation for this observation could be linked to distinct cell cycle duration among the different cell types. Live-imaging experiments indicate a shorter cell cycle duration for stele cells (*c.* 15 h) compared with other root cell types (*c.* 23 h for cortex and 24 h for the epidermis)

(Rahni & Birnbaum, 2019). Faster proliferation rates have been correlated with increased susceptibility to DNA damage (Kiraly *et al.*, 2015; Alhmoud *et al.*, 2020). Notably, stele cells have demonstrated higher sensitivity to cell death in response to zeocin (Yoshiyama *et al.*, 2017; Johnson *et al.*, 2018; Ryu *et al.*, 2019). Consequently, the greater accumulation of damage may underscore the elevated transcriptional response of *RAD51* in stele cells.

The observation of *RAD51* transcription occurring outside S/G2 phases of the cell cycle is another important finding of this study. DDR via HR and *RAD51* gene expression has been associated with S and G2 phases of the cell cycle in many organisms (Basile *et al.*, 1992; Yamamoto *et al.*, 1996; Doutriaux *et al.*, 1998). In Arabidopsis, *RAD51* transcription in response to DNA damage was coincident with the cell cycle arrest at G2/M checkpoint (Osakabe *et al.*, 2005; De Schutter *et al.*, 2007). Later studies demonstrated that both G1/S and G2/M checkpoints can be used to ensure cell cycle arrest in response to DNA damage. For example, hydroxyurea (HU) treatment was shown to activate both G2/M cell cycle arrest (De Schutter *et al.*, 2007) and G1/S checkpoint (Saban & Bujak, 2009; Cabral *et al.*, 2020), a phenomenon also observed in response to gamma irradiation (Hefner, 2003; Hefner *et al.*, 2006; Ricaud *et al.*, 2007). Zeocin, the radiomimetic drug used in this study to induce DSBs, was so far reported to promote arrest at the G2/M and G1/S checkpoints (De Schutter *et al.*, 2007; Adachi *et al.*, 2011; Chen *et al.*, 2017).

In this study, we used marker lines for evaluation of the cell cycle in response to zeocin treatment. However, it is crucial to acknowledge that DNA damage may directly impact the expression of reporter genes (Weimer *et al.*, 2016). For instance, the G2/M-marker gene *CYCB1;1* was previously shown to be responsive to DNA damage (Culligan *et al.*, 2006). Therefore, caution is required when interpreting the data. We have evaluated cell cycle progression using different lines as well as reporter-independent approaches, and our findings suggest that cells are undergoing arrest at both G1/S and G2/M checkpoints in response to zeocin treatment with large proportion of G1/S cells. Importantly, our data suggest that *RAD51* can be also transcribed in G1 phase. Previous studies propose a potential reason and implication behind the release of the S/G2 restriction of *RAD51* expression. For instance, it was shown that repetitive sequences can be repaired via HR during G1 phase, proven by the recruitment of RAD51 to centromeric break sites in mouse and human cells (Yilmaz *et al.*, 2021). The HR machinery is also involved in G1 repair of ribosomal DNA, another type of repetitive sequence in human cell cultures (van Sluis & McStay, 2015). Moreover, non-recombinogenic functions in DNA repair were suggested for RAD51 and some HR proteins (Cano-Linares *et al.*, 2021; Prado, 2021). We suggest this as one of the potential reasons behind our observation of active *RAD51* transcription in G1 after DNA damage exposure. Also, in Arabidopsis, RAD54 foci were shown to emerge with high frequency in both in G1 and G2 cells after gamma irradiation (Hirakawa & Matsunaga, 2019). The necessity of prior RAD51 foci formation for the formation of RAD54 foci points to the possibility of RAD51 foci presence in G1 phase Arabidopsis cells (Hirakawa *et al.*, 2017).

Altogether, the results of this article shed new light on the DNA damage response in plants, uncovering distinctions in the transcriptional response of *RAD51* across various cell types. Moreover, it highlights the noteworthy occurrence of transcription during the G1 phase of the cell cycle.

Acknowledgements

Competing interests

None declared.

Author contributions

KK, S Reeck, AM, AS, CW and S Rosa designed the research. KK performed the research and data analysis. AF assisted data analysis and created software pipelines for image analysis. KS assisted statistical analysis of the data. KK and S Rosa wrote the manuscript. CW provided material for the study. S Reeck, AM, CW and AS critically read the manuscript.

ORCID

Alejandro Fonseca https://orcid.org/0000-0002-1696-7385
Konstantin Kutashev https://orcid.org/0000-0002-1563-5303
Anis Meschichi https://orcid.org/0000-0001-8946-6023
Svenja Reeck https://orcid.org/0000-0002-6362-5310
Stefanie Rosa https://orcid.org/0000-0002-8100-1253
Kevin Sartori https://orcid.org/0000-0001-7364-1341
Adrien Sicard https://orcid.org/0000-0002-4104-6844
Charles I. White https://orcid.org/0000-0001-8152-5797

Data availability

All the raw microscopy images used in this manuscript are openly available at doi: 10.5061/dryad.9w0vt4bq3.

References

Abe K, Osakabe K, Nakayama S, Endo M, Tagiri A, Todoriki S, Ichikawa H, Toki S. 2005. Arabidopsis Rad51c gene is important for homologous recombination in meiosis and mitosis. *Plant Physiology* 139: 896–908.

Adachi S, Minamisawa K, Okushima Y, Inagaki S, Yoshiyama K, Kondou Y, Kaminuma E, Kawashima M, Toyoda T, Matsui M *et al.* 2011. Programmed induction of endoreduplication by DNA double-strand breaks in *Arabidopsis*. *Proceedings of the National Academy of Sciences, USA* 108: 10004–10009.

Aki S, Umeda M. 2016. Cytrap marker systems for *in vivo* visualization of cell cycle progression in Arabidopsis. In: Caillaud M-C, ed. *Methods in molecular biology. Plant cell division*. New York, NY, USA: Springer, 51–57.

Alhmoud J, Woolley J, Al Moustafa A-E, Malki M. 2020. DNA damage/repair management in cancers. *Cancers* 12: 1050.

Banerjee S, Roy S. 2021. An insight into understanding the coupling between homologous recombination mediated DNA repair and chromatin remodeling mechanisms in plant genome: an update. *Cell Cycle* 20: 1760–1784.

Basile G, Aker M, Mortimer R. 1992. Nucleotide sequence and transcriptional regulation of the yeast recombinational repair gene Rad51. *Molecular and Cellular Biology* 12: 3235–3246.

Bee L, Fabris S, Cherubini R, Mognato M, Celotti L. 2013. The efficiency of homologous recombination and non-homologous end joining systems in repairing double-strand breaks during cell cycle progression. *PLoS ONE* 8: E69061.

Biedermann S, Harashima H, Chen P, Heese M, Bouyer D, Sofroni K, Schnittger A. 2017. The retinoblastoma homolog RBR 1 mediates localization of the repair protein RAD 51 to DNA lesions in *Arabidopsis*. *EMBO Journal* 36: 1279–1297.

Bonilla B, Sr H, Mk G, Ka B. 2020. *Rad51* gene family structure and function. *Annual Review of Genetics* 54: 25–46.

Cabral D, My B, Antonino J, Rodiuc N, Vieira P, Rr C, Chevalier C, Eekhout T, Engler G, De Veylder L *et al.* 2020. The plant Wee1 kinase is involved in checkpoint control activation in nematode-induced galls. *New Phytologist* 225: 430–447.

Cano-Linares M, Yáñez-Vilches A, García-Rodríguez N, Barrientos-Moreno M, González-Prieto R, San-Segundo P, Ulrich H, Prado F. 2021. Non-recombinogenic roles for Rad52 in translesion synthesis during DNA damage tolerance. *EMBO Reports* 22: E50410.

Chabot T, Defontaine A, Marquis D, Renodon-Corniere A, Courtois E, Fleury F, Cheraud Y. 2019. New phosphorylation sites of Rad51 by C-met modulates presynaptic filament stability. *Cancers* 11: 413.

Charbonnel C, Me G, Ci W. 2010. Xrcc1-dependent and ku-dependent DNA double-strand break repair kinetics in Arabidopsis plants: double-strand break repair kinetics in Arabidopsis. *The Plant Journal* 64: 280–290.

Chen P, Takatsuka H, Takahashi N, Kurata R, Fukao Y, Kobayashi K, Ito M, Umeda M. 2017. Arabidopsis R1r2r3-Myb proteins are essential for inhibiting cell division in response to DNA damage. *Nature Communications* 8: 635.

Coïc E, Martin J, Ryu T, Sy T, Kondev J, Je H. 2011. Dynamics of homology searching during gene conversion in *Saccharomyces cerevisiae* revealed by donor competition. *Genetics* 189: 1225–1233.

Cools T, Iantcheva A, Ak W, Boens S, Takahashi N, Maes S, Van Den Daele H, Van Isterdael G, Schnittger A, De Veylder L. 2011. The *Arabidopsis thaliana* checkpoint kinase wee1 protects against premature vascular differentiation during replication stress. *Plant Cell* 23: 1435–1448.

Cui W, Wang H, Song J, Cao X, Hj R, Francis D, Jia C, Sun L, Hou M, Yang Y *et al.* 2017. Cell cycle arrest mediated by cd-induced dna damage in arabidopsis root tips. *Ecotoxicology and Environmental Safety* 145: 569–574.

Culligan K, Robertson C, Foreman J, Doerner P, Britt A. 2006. ATR and ATM play both distinct and additive roles in response to ionizing radiation. *The Plant Journal* 48: 947–961.

Da Ines O, Bazile J, Gallego M, White C. 2022. Dmc1 attenuates Rad51-mediated recombination in arabidopsis. *PLoS Genetics* 18: E1010322.

Da Ines O, Degroote F, Goubely C, Amiard S, Gallego M, White C. 2013. Meiotic recombination in arabidopsis is catalysed by Dmc1, with Rad51 playing a supporting role. *PLoS Genetics* 9: E1003787.

De Schutter K, Joubès J, Cools T, Verkest A, Corellou F, Babiychuk E, Van Der Schueren E, Beeckman T, Kushnir S, Inzé D *et al.* 2007. Arabidopsis Wee1 kinase controls cell cycle arrest in response to activation of the DNA integrity checkpoint. *Plant Cell* 19: 211–225.

Desvoyes B, Arana-Echarri A, Barea M, Gutierrez C. 2020. A comprehensive fluorescent sensor for spatiotemporal cell cycle analysis in arabidopsis. *Nature Plants* 6: 1330–1334.

Desvoyes B, Noir S, Masoud K, Mi L, Genschik P, Gutierrez C. 2019. Fbl17 targets Cdt1a for degradation in early S-Phase to prevent Arabidopsis genome instability. *BioRxiv*. doi: 10.1101/774109.

Doutriaux M-P, Couteau F, Bergounioux C, White C. 1998. Isolation and characterisation of the Rad51 and Dmc1 homologs from *Arabidopsis thaliana*. *Molecular and General Genetics MGG* **257**: 283–291.

Duncan S, Olsson T, Hartley M, Dean C, Rosa S. 2017. Single molecule RNA fish in arabidopsis root cells. *Bio-Protocol* **7**: e2240.

Duncan S, Olsson T, Hartley M, Dean C, Rosa S. 2016. A method for detecting single mRNA molecules in *Arabidopsis thaliana*. *Plant Methods* **12**: 13.

Fan T, Kang H, Wu D, Zhu X, Huang L, Wu J, Zhu Y. 2022. Arabidopsis γ-H2AX-interacting protein participates in DNA damage response and safeguards chromatin stability. *Nature Communications* **13**: 7942.

Feng W, Hale CJ, Over RS, Cokus SJ, Jacobsen SE, Michaels SD. 2017. Large-scale heterochromatin remodeling linked to overreplication-associated DNA damage. *Proceedings of the National Academy of Sciences, USA* **114**: 406–411.

Flott S, Kwon Y, Yz P, Pa R, Sung P, Sp J. 2011. Regulation of Rad51 function by phosphorylation. *EMBO Reports* **12**: 833–839.

Friesner J, Liu B, Culligan K, Britt A. 2005. Ionizing radiation–dependent γ-H2AX focus formation requires ataxia telangiectasia mutated and ataxia telangiectasia mutated and Rad3-related. *Molecular Biology of the Cell* **16**: 2566–2576.

Fulcher N, Sablowski R. 2009. Hypersensitivity to DNA damage in plant stem cell niches. *Proceedings of the National Academy of Sciences, USA* **106**: 20984–20988.

Gamborg O, Murashige T, Thorpe T, Vasil I. 1976. Plant tissue culture media. *In Vitro* **12**: 473–478.

Goldfarb T, Lichten M. 2010. Frequent and efficient use of the sister chromatid for DNA double-strand break repair during budding yeast meiosis. *PLoS Biology* **8**: E1000520.

Hefner E. 2003. Arabidopsis mutants sensitive to gamma radiation include the homologue of the human repair gene Ercc1. *Journal of Experimental Botany* **54**: 669–680.

Hefner E, Huefner N, Ab B. 2006. Tissue-specific regulation of cell-cycle responses to DNA damage in Arabidopsis seedlings. *DNA Repair* **5**: 102–110.

Hicks W, Yamaguchi M, Haber J. 2011. Real-time analysis of double-strand DNA break repair by homologous recombination. *Proceedings of the National Academy of Sciences, USA* **108**: 3108–3115.

Hirakawa T, Hasegawa J, Ci W, Matsunaga S. 2017. RAD 54 forms DNA repair foci in response to DNA damage in living plant cells. *The Plant Journal* **90**: 372–382.

Hirakawa T, Matsunaga S. 2019. Characterization of DNA repair foci in root cells of Arabidopsis in response to DNA damage. *Frontiers in Plant Science* **10**: 990.

Johnson R, Conklin P, Tjahjadi M, Missirian V, Toal T, Brady S, Britt A. 2018. Suppressor of gamma response1 links DNA damage response to organ regeneration. *Plant Physiology* **176**: 1665–1675.

Johnson R. 2000. Sister chromatid gene conversion is a prominent double-strand break repair pathway in mammalian cells. *EMBO Journal* **19**: 3398–3407.

Kiraly O, Gong G, Olipitz W, Muthupalani S, Engelward B. 2015. Inflammation-induced cell proliferation potentiates DNA damage-induced mutations *in vivo*. *PLoS Genetics* **11**: E1004901.

Lang J, Smetana O, Sanchez-Calderon L, Lincker F, Genestier J, Schmit A, Houlné G, Chabouté M. 2012. Plant γH2AX foci are required for proper DNA DSB repair responses and colocalize with E2f factors. *New Phytologist* **194**: 353–363.

Lee Y, Wang Q, Shuryak I, Brenner D, Turner H. 2019. Development of a high-throughput γ-H2AX assay based on imaging flow cytometry. *Radiation Oncology* **14**: 150.

Li W, Chen C, Markmann-Mulisch U, Timofejeva L, Schmelzer E, Ma H, Reiss B. 2004. The Arabidopsis Atrad51 gene is dispensable for vegetative development but required for meiosis. *Proceedings of the National Academy of Sciences, USA* **101**: 10596–10601.

Lim D-S, Hasty P. 1996. A mutation in mouse *Rad51* results in an early embryonic lethal that is suppressed by a mutation in *P53*. *Molecular and Cellular Biology* **16**: 7133–7143.

Lim G, Chang Y, Huh W-K. 2020. Phosphoregulation of Rad51/Rad52 by Cdk1 functions as a molecular switch for cell cycle–specific activation of homologous recombination. *Science Advances* **6**: Eaay2669.

Löbrich M, Shibata A, Beucher A, Fisher A, Ensminger M, Goodarzi A, Barton O, Jeggo P. 2010. γH2AX foci analysis for monitoring DNA double-strand break repair: strengths, limitations and optimization. *Cell Cycle* **9**: 662–669.

Meschichi A, Zhao L, Reeck S, White C, Da Ines O, Sicard A, Pontvianne F, Rosa S. 2022. The plant-specific DDR factor sog1 increases chromatin mobility in response to DNA damage. *EMBO Reports* **23**: E54736.

Mueller F, Senecal A, Tantale K, Marie-Nelly H, Ly N, Collin O, Basyuk E, Bertrand E, Darzacq X, Zimmer C. 2013. Fish-quant: automatic counting of transcripts in 3d fish images. *Nature Methods* **10**: 277–278.

Muschel R, Zhang H, Iliakis G, Mckenna W. 1991. Cyclin B expression in hela cells during the G2 block induced by ionizing radiation. *Cancer Research* **51**: 5113–5117.

Musielak T, Schenkel L, Kolb M, Henschen A, Bayer M. 2015. A simple and versatile cell wall staining protocol to study plant reproduction. *Plant Reproduction* **28**: 161–169.

Narsai R, Howell K, Millar A, O'toole N, Small I, Whelan J. 2007. Genome-wide analysis of mRNA decay rates and their determinants in *Arabidopsis thaliana*. *Plant Cell* **19**: 3418–3436.

Osakabe K, Abe K, Yamanouchi H, Takyuu T, Yoshioka T, Ito Y, Kato T, Tabata S, Kurei S, Yoshioka Y et al. 2005. Arabidopsis Rad51b is important for double-strand DNA breaks repair in somatic cells. *Plant Molecular Biology* **57**: 819–833.

Prado F. 2021. Non-recombinogenic functions of RAD51, BRCA2, And RAD52 in DNA damage tolerance. *Genes* **12**: 1550.

Preuss S, Britt A. 2003. A DNA-damage-induced cell cycle checkpoint in Arabidopsis. *Genetics* **164**: 323–334.

Rahni R, Birnbaum K. 2019. Week-long imaging of cell divisions in the Arabidopsis root meristem. *Plant Methods* **15**: 30.

Raj A, Van Den Bogaard P, Rifkin S, Van Oudenaarden A, Tyagi S. 2008. Imaging individual mRNA molecules using multiple singly labeled probes. *Nature Methods* **5**: 877–879.

Raleigh J, O'connell M. 2000. The G2 DNA damage checkpoint targets both Wee1 and Cdc25. *Journal of Cell Science* **113**: 1727–1736.

Redon C, Dickey J, Bonner W, Sedelnikova O. 2009. γ-H2AX as a biomarker of DNA damage induced by ionizing radiation in human peripheral blood lymphocytes and artificial skin. *Advances in Space Research* **43**: 1171–1178.

Ricaud L, Proux C, Renou J-P, Pichon O, Fochesato S, Ortet P, Montané M-H. 2007. ATM-mediated transcriptional and developmental responses to γ-rays in Arabidopsis. *PLoS ONE* **2**: E430.

Rogakou E, Boon C, Redon C, Bonner W. 1999. Megabase chromatin domains involved in DNA double-strand breaks *in vivo*. *The Journal of Cell Biology* **146**: 905–916.

Ryu T, Ys G, Choi S, Kim J, By C, Kim J. 2019. SOG 1-dependent NAC 103 modulates the DNA damage response as a transcriptional regulator in Arabidopsis. *The Plant Journal* **98**: 83–96.

Saban N, Bujak M. 2009. Hydroxyurea and hydroxamic acid derivatives as antitumor drugs. *Cancer Chemotherapy and Pharmacology* **64**: 213–221.

Saintigny Y, Delacôte F, Boucher D, Averbeck D, Bs L. 2007. Xrcc4 in G1 suppresses homologous recombination in S/G2, in G1 checkpoint-defective cells. *Oncogene* **26**: 2769–2780.

Saleh-Gohari N. 2004. Conservative homologous recombination preferentially repairs DNA double-strand breaks in the S phase of the cell cycle in human cells. *Nucleic Acids Research* **32**: 3683–3688.

Salic A, Mitchison T. 2008. A chemical method for fast and sensitive detection of DNA synthesis *in vivo*. *Proceedings of the National Academy of Sciences, USA* **105**: 2415–2420.

Schuermann D, Molinier J, Fritsch O, Hohn B. 2005. The dual nature of homologous recombination in plants. *Trends in Genetics* **21**: 172–181.

Shinohara A, Ogawa H, Ogawa T. 1992. RAD51 protein involved in repair and recombination in S. cerevisiae is a RecA-like protein. *Cell* **69**: 457–470.

Sørensen C, Hansen L, Dziegielewski J, Syljuåsen R, Lundin C, Bartek J, Helleday T. 2005. The cell-cycle checkpoint kinase Chk1 is required for mammalian homologous recombination repair. *Nature Cell Biology* **7**: 195–201.

Sorenson R, Deshotel M, Johnson K, Adler F, Sieburth L. 2018. *Arabidopsis* mRNA decay landscape arises from specialized RNA decay substrates,

decapping-mediated feedback, and redundancy. *Proceedings of the National Academy of Sciences, USA* 115: E1485–E1494.

Stewart G, Wang B, Bignell C, Taylor A, Elledge S. 2003. Mdc1 is a mediator of the mammalian DNA damage checkpoint. *Nature* 421: 961–966.

Stirling D, Swain-Bowden M, Lucas A, Carpenter A, Cimini B, Goodman A. 2021. CELLPROFILER 4: improvements in speed, utility and usability. *BMC Bioinformatics* 22: 433.

Stringer C, Wang T, Michaelos M, Pachitariu M. 2021. Cellpose: a generalist algorithm for cellular segmentation. *Nature Methods* 18: 100–106.

Su H, Cheng Z, Huang J, Lin J, Gp C, Ma H, Wang Y. 2017. Arabidopsis Rad51, Rad51c and Xrcc3 proteins form a complex and facilitate Rad51 localization on chromosomes for meiotic recombination. *PLoS Genetics* 13: E1006827.

Takahashi N, Ogita N, Takahashi T, Taniguchi S, Tanaka M, Seki M, Umeda M. 2019. A regulatory module controlling stress-induced cell cycle arrest in Arabidopsis. *eLife* 8: E43944.

Tsuzuki T, Fujii Y, Sakumi K, Tominaga Y, Nakao K, Sekiguchi M, Matsushiro A, Yoshimura Y, Moritat S. 1996. Targeted disruption of the rad51 gene leads to lethality in embryonic mice. *Proceedings of the National Academy of Sciences, USA* 93: 6236–6240.

Van Sluis M, Mcstay B. 2015. A localized nucleolar DNA damage response facilitates recruitment of the homology-directed repair machinery independent of cell cycle stage. *Genes & Development* 29: 1151–1163.

Vítor A, Huertas P, Legube G, De Almeida S. 2020. Studying DNA double-strand break repair: an ever-growing toolbox. *Frontiers in Molecular Biosciences* 7: 24.

Wang S, Durrant W, Song J, Spivey N, Dong X. 2010. *Arabidopsis* Brca2 and Rad51 proteins are specifically involved in defense gene transcription during plant immune responses. *Proceedings of the National Academy of Sciences, USA* 107: 22716–22721.

Wang Y, Xiao R, Wang H, Cheng Z, Li W, Zhu G, Wang Y, Ma H. 2014. The Arabidopsis Rad51 paralogs Rad51b, Rad51d and Xrcc2 play partially redundant roles in somatic dna repair and gene regulation. *New Phytologist* 201: 292–304.

Weimer A, Biedermann S, Harashima H, Roodbarkelari F, Takahashi N, Foreman J, Guan Y, Pochon G, Heese M, Van Damme D *et al.* 2016. The plant-specific CDKB 1- CYCB 1 complex mediates homologous recombination repair in *Arabidopsis*. *EMBO Journal* 35: 2068–2086.

West C, Waterworth W, Sunderland P, Bray C. 2004. *Arabidopsis* DNA double-strand break repair pathways. *Biochemical Society Transactions* 32: 964–966.

Woo T-T, Chuang C-N, Higashide M, Shinohara A, Wang T-F. 2020. Dual roles of yeast Rad51 N-terminal domain in repairing DNA double-strand breaks. *Nucleic Acids Research* 48: 8474–8489.

Woo T-T, Chuang C-N, Wang T-F. 2021. Budding yeast Rad51: a paradigm for how phosphorylation and intrinsic structural disorder regulate homologous recombination and protein homeostasis. *Current Genetics* 67: 389–396.

Yamamoto A, Yagi H, Habu T, Yoshimura Y, Matsushiro A, Nishimune Y, Morita T, Taki T, Yoshida K, Yamamoto K *et al.* 1996. Cell cycle-dependent expression of the mouse Rad51 gene in proliferating cells. *Molecular and General Genetics* 251: 1–12.

Yata K, Lloyd J, Maslen S, Bleuyard J-Y, Skehel M, Smerdon S, Esashi F. 2012. Plk1 and Ck2 act in concert to regulate Rad51 during DNA double strand break repair. *Molecular Cell* 45: 371–383.

Yilmaz D, Furst A, Meaburn K, Lezaja A, Wen Y, Altmeyer M, Reina-San-Martin B, Soutoglou E. 2021. Activation of homologous recombination in G1 preserves centromeric integrity. *Nature* 600: 748–753.

Yin K, Ueda M, Takagi H, Kajihara T, Sugamata Aki S, Nobusawa T, Umeda-Hara C, Umeda M. 2014. A dual-color marker system for *in vivo* visualization of cell cycle progression in Arabidopsis. *The Plant Journal* 80: 541–552.

Yoshiyama K, Kaminoyama K, Sakamoto T, Kimura S. 2017. Increased phosphorylation of ser-gln sites on suppressor of gamma response1 strengthens the DNA damage response in *Arabidopsis thaliana*. *Plant Cell* 29: 3255–3268.

Yu C, Hou L, Huang Y, Cui X, Xu S, Wang L, Yan S. 2023. The MULTI-BRCT domain protein DDRM2 promotes the recruitment of RAD51 to DNA damage sites to facilitate homologous recombination. *New Phytologist* 238: 1073–1084.

Zhao L, Fonseca A, Meschichi A, Sicard A, Rosa S. 2023. Whole-mount smfish allows combining RNA and protein quantification at cellular and subcellular resolution. *Nature Plants* 9: 1094–1102.

Supporting Information

Additional Supporting Information may be found online in the Supporting Information section at the end of the article.

Fig. S1 Evaluation of *RAD51* and *PP2A* transcription in response to growing amounts of DNA damage.

Fig. S2 Quantification of *RAD51* transcription sites and mRNAs per cell from Arabidopsis (Col-0) roots using whole-mount single-molecule RNA fluorescence *in situ* hybridization.

Fig. S3 Quantification of *RAD51* mRNA molecules in Arabidopsis roots exposed to increasing amounts of DNA damage using whole-mount single-molecule RNA fluorescence *in situ* hybridization.

Fig. S4 Magnified representative images from Arabidopsis root cells with different number of *RAD51* mRNAs obtained by whole-mount single-molecule RNA fluorescence *in situ* hybridization.

Fig. S5 Quantification of *RAD51* mRNA molecules per cell in stem cells of Arabidopsis roots.

Fig. S6 Evaluation of *Arabidopsis thaliana* Col-0 seedling recovery following a 12-h exposure to various concentrations of zeocin.

Fig. S7 *RAD51* transcriptional response in meristematic and elongation zones of Arabidopsis roots using whole-mount single-molecule RNA fluorescence *in situ* hybridization.

Fig. S8 Quantification of *RAD51-GFP* mRNA and RAD51-GFP protein signals in roots of Arabidopsis RAD51-GFP line treated with 0 and 10 μM zeocin.

Fig. S9 Quantification of *RAD51-GFP* mRNA and RAD51-GFP protein signals in roots of Arabidopsis RAD51-GFP line treated with 50 μM of zeocin.

Fig. S10 Quantification of *RAD51-GFP* mRNA and RAD51-GFP protein signals in roots of Arabidopsis RAD51-GFP line treated with 170 μM of zeocin.

Fig. S11 Evaluation of cell cycle arrest in Arabidopsis roots using 5-ethynyl-2 ′-deoxyuridine staining.

Fig. S12 Evaluation of cell cycle changes using Cytrap line in roots after exposure different concentrations of zeocin.

Fig. S13 Quantification of DAPI signal intensity in Arabidopsis roots exposed to different concentrations of zeocin.

Fig. S14 Evaluation of cell cycle changes using PlaCCI line in roots after exposure to different concentrations of zeocin.

Fig. S15 Assessment of *RAD51* mRNA molecule half-life.

Fig. S16 Quantification of *RAD51* mRNAs cell in cells with and without 5-ethynyl-2 $'$-deoxyuridine staining.

Table S1 smFISH probe sequences used in this study and the corresponding dyes.

Table S2 *RAD51* transcription site quantification in cells residing at G1 vs other phases of the cell cycle using CDT1-CFP line in Arabidopsis roots.

Please note: Wiley is not responsible for the content or functionality of any Supporting Information supplied by the authors. Any queries (other than missing material) should be directed to the *New Phytologist* Central Office.

RIGHTSLINK
Copyright Clearance Center